

POLARIZATION OBSERVATIONS OF 100 PULSARS AT 774 MHZ BY THE GREEN BANK TELESCOPE

J. L. HAN¹, P. B. DEMOREST², W. VAN STRATEN³, A. G. LYNE⁴

Received 2008 September 16; accepted 2009 January 9; published 2009 March 24. ApJS 181:557-571 doi:10.1088/0067-0049/181/2/557

ABSTRACT

We report on polarimetric observations of 100 pulsars centered on 774 MHz, made using the Green Bank Telescope, presenting their polarization profiles and polarized flux densities and comparing them with previous observations when possible. For 67 pulsars, these are the first such measurements made. Polarization profiles of 8 millisecond pulsars in our sample show wide profiles and flat position-angle curves. Strong linear polarization, sometimes approaching 100% of the total intensity, has been detected in all or a part of the average pulse profiles of some pulsars. In general, circular polarization is very weak, although it is observed to be extremely strong in the leading component of PSR J1920+2650. Sense reversal of circular polarization as a function of pulse phase has been detected from both core and other components of more than 20 pulsars. Any relationship between the spin-down luminosity and the percentage of linear polarization is not evident in our data at this frequency.

Subject headings: Pulsars: general

1. INTRODUCTION

More than 40 years after the discovery of the first pulsars, there is currently no consensus on how electromagnetic radiation is generated in the pulsar magnetosphere. Soon after their discovery, it was observed that the radio emission from pulsars is highly polarized (Lyne & Smith 1968), with the linearly polarized fraction approaching 100% in some or all profile components. Some pulsars also have prominent circular polarization (see a summary by Han et al. 1998). Observations of pulsar polarization continue to provide new insights into the emission mechanism (e.g. Lyne & Manchester 1988; Rankin 1993).

Pulse profiles tend to have many peaks, which are related to the brightness distribution inside the pulsar radiation beam. Rankin (1983, 1993) suggested that pulsar emission beams consist of two distinct component types: a central core surrounded by one or more hollow cones. The cones in such a beam tend to be shifted to earlier longitudes with respect to the center of the core (Gupta & Gangadhara 2003). We note that the conventional model with one core plus two cones cannot explain more than five components: e.g. greater than six components for PSR B0740-28 (Kramer 1994), nine components for PSR B0329+54 (Gangadhara & Gupta 2001), greater than 13 components for PSR J0437-4715 (Navarro et al. 1997) and PSR J2124-3358 (Manchester & Han 2004). A model with a multiconal beam has been proposed for some pulsars (Gangadhara & Gupta 2001). A pulsar emission beam filled with “randomly” distributed emission patches (Lyne & Manchester 1988; Han & Manchester 2001) may explain more complicated multicomponent profiles.

Pulsar emission is thought to come from two possible regions, one near the magnetic poles and the other near the light cylinder (e.g. Ruderman & Sutherland 1975; Cheng et al. 1986; Zhang & Harding 2000). It is also possible that the radio or high-energy emission is radiated by particles flowing from the poles all the way to the light-cylinder (e.g. Gangadhara & Gupta 2001; Gupta & Gangadhara 2003; Qiao et al. 2004). Backward-flowing particles may also contribute to the observed radio emis-

sion (Dyks et al. 2005). Different components may originate at different altitudes (Karastergiou & Johnston 2007) and/or from different magnetic field lines, and the core component is probably emitted at a lower altitude (Gil 1991).

At a given rotational phase, the polarization angle (P.A.) of the observed linear polarization is thought to be related to the plane of curved magnetic field lines tangential to the line of sight (LOS) in the neutron star magnetosphere. In the ideal case, the P.A. curve of the on-pulse phases follows the “S”-shape of the “rotating vector model” (Radhakrishnan & Cooke 1969). This model was confirmed by the earliest observations of some pulsars, which led to the long-term belief that the radio emission is generated only near the magnetic poles.

Radio emission generated at higher altitudes (Manchester 1996; Johnston & Weisberg 2006), even near the light cylinder, should produce a flatter P.A. curve, and suffer less from propagation effects in the magnetosphere. To date, flat P.A. curves for just one component together with the “S”-shaped P.A. for other components have been observed for many pulsars, which may indicate that different components originate at different emission altitudes. That is to say, even the emission at a single frequency may come from different regions in the neutron star magnetosphere.

Millisecond pulsars have much smaller light cylinders than normal pulsars, so that the emission region is limited to a magnetosphere that is 6 or 7 orders of magnitude smaller in volume. The total intensity profiles of millisecond pulsars are qualitatively similar to those of normal pulsars, though with a tendency to cover a wider region of pulse phase (Kramer et al. 1998). In contrast, the polarization profiles of millisecond pulsars (Xilouris et al. 1998; Stairs et al. 1999; Manchester & Han 2004; Ord et al. 2004) are typically much more complex than those of normal pulsars. Polarization observations of millisecond pulsars are relatively scarce, and most are presently available at only one radio frequency (see references above).

Single pulse polarization observations show that orthogonal modes of polarization can be emitted at a given pulse phase (Stinebring et al. 1984a; McKinnon & Stinebring 2000). In the integrated polarization profile, transitions between orthogonal modes typically stand out as jumps in the P.A. curve; in general, orthogonally polarized modes are elliptically polarized (Cordes et al. 1978; McKinnon 2004). Furthermore, histograms of the orientation of the polarization vector provide evidence of nonorthogonal modes of emission at a given pulse longitude (Edwards & Stappers

¹ National Astronomical Observatories, Chinese Academy of Sciences, Jia 20 DaTun Road, Beijing 100012, China

² National Radio Astronomy Observatory, Charlottesville, VA 22903, USA

³ Centre for Astrophysics and Supercomputing, Swinburne University of Technology, PO Box 218, Hawthorn, VIC 3122, Australia

⁴ University of Manchester, Jodrell Bank Observatory, Macclesfield, SK11, 9DL, UK

2004).

We have observed 100 pulsars with the Green Bank Telescope (GBT) in order to measure their polarization properties. We also determined the rotation measures (RMs) of these pulsars. The RMs will be presented in a second paper (Han et al. 2008), and, together with an additional 377 RMs, will be used in an analysis of the large-scale Galactic magnetic field. In this paper, we present the polarization profiles and polarized flux densities obtained for these pulsars, beginning with a description of the observations in Section 2. In Section 3, the polarization profiles are grouped according to similar characteristics. In Section 4, the results are summarized, and the dependence of polarization percentage on the rotational energy loss rate (\dot{E}) is discussed.

2. OBSERVATIONS

Pulsar polarization observations were carried out with the NRAO GBT⁹ between 2007 November 17 and 26, using the 800 MHz prime focus receiver. This dual-polarization receiver amplifies the signals from two linear receptors, X and Y , using cooled field-effect transistors. The choice of central observation frequency, 774 MHz, was primarily based on the absence of significant radio frequency interference. The amplified RF signals were mixed to an intermediate frequency of 400 MHz then fed into the Green Bank Astronomy Signal Processor (GASP) pulsar backend (Demorest 2007; Ferdman et al. 2004). In the GASP system, 128 MHz total bandwidth was sampled in each polarization and then divided into 32 4-MHz subbands in hardware using a digital polyphase filter bank. The 4-MHz subbands were distributed to a 16-node computer cluster for additional real-time software signal processing. In this case, the signal was divided further in frequency for a final spectral resolution of 0.25 MHz. The X and Y signals in each channel were detected and cross-multiplied to form the coherency products XX , YY , X^*Y , and XY^* . These values were later converted to Stokes parameters during the calibration process via a simple linear transformation, as described by van Straten (2004).

The coherency products in each channel were averaged or folded (also in real time) into 1024 pulse-phase bins modulo the predicted apparent pulse period of each source. Pulsar ephemerides were obtained from the ATNF Pulsar Catalog (Manchester et al. 2005), with the exception of 25 sources where new timing data from Jodrell Bank were used instead. All ephemerides were processed with the pulsar analysis program TEMPO¹⁰. The folded profiles were saved in 30 s subintegrations using the standard PSRFITS data format (Hotan et al. 2004).

The computation-limited real-time processing allowed us to record a total bandwidth of 96 MHz (384 channels) covering the range from 726 to 822 MHz, resulting in an effective central observation frequency of 774 MHz. Due to aliasing effects and strong instrumental polarization, the edge channels within each 4 MHz subband were flagged and ignored in our subsequent analysis. There are also two receiver resonances in this band, one at 796.6 MHz with a 2.1 MHz bandwidth, and the other at 817 MHz with a 3.3 MHz bandwidth. Channels in these regions were also ignored, resulting in a total (discontinuous) usable bandwidth of ~ 80 MHz.

Before observing any pulsars, the overall system gain was

⁹ The National Radio Astronomy Observatory is a facility of the National Science Foundation operated under cooperative agreement by Associated Universities, Inc.

¹⁰ see <http://www.atnf.csiro.au/research/pulsar/tempo/>

calibrated by observing the flux calibrators 3C286 and 3C295. A low-level (4 K) calibration signal (cal) produced by a noise diode that is coupled to the X and Y receptors before the primary amplifier was switched on and off at 25 Hz. This nominally linearly polarized cal signal was recorded for 4*30 s (i.e. 4 separate recordings of 30 s; the same notation is used below) by GASP while pointing at each flux calibrator. The levels of all signals were adjusted using attenuators to preserve linearity of the system. The telescope was then pointed at a position 2° away from each flux calibrator and the pulsed cal signal was recorded again. These two data sets were used to determine the flux density of the cal signal relative to 3C286 and 3C295, whose flux densities at 800 MHz were calculated according to Baars et al. (1977).

The cal was reobserved prior to observing each pulsar. The telescope was pointed at a position 15' offset from the pulsar (15' is the FWHM telescope beam size at 800 MHz), and the pulsed cal was recorded for 2*30 s. The pulsar was then observed with the cal signal turned off, and observed the pulsar as described above for 8*30 s. The GBT prime focus receivers are located on a focus rotation mount on a retractable boom. We took advantage of this feature by rotating the whole receiver by 90°, and re-observing the pulsar for another 8*30 s. The addition of the two data sets reduces the error in Stokes Q that arises from the experimental uncertainty in the differential gain calibration.

Data reduction and polarimetric calibration were performed using PSRCHIVE (Hotan et al. 2004). First, we plotted the data in each subintegration and frequency channel and manually removed any obvious interference. Second, we obtained the receiver cross-coupling parameters from observations of PSR B1929+10 at several different hour angles (van Straten 2004); the best-fit

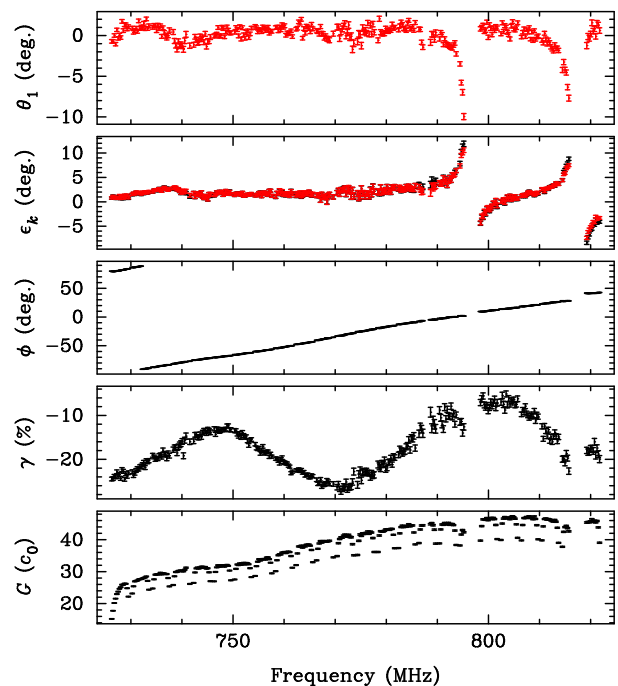


FIG. 1.— Best-fit instrumental parameters as a function of observing frequency. From top to bottom are plotted the nonorthogonality, θ_1 , and ellipticities, ϵ_k , of the feed receptors, the differential phase, ϕ , the differential gain ratio, γ , and the absolute gain, G . The receiver resonances at 796.6 MHz and 817 MHz are clearly seen as discontinuities in receptor ellipticity and orthogonality estimates.

solution is shown in Figure 1. Third, as described by Ord et al. (2004), we calibrated the pulsar data using a combination of the instrumental polarization solution, the flux density calibration information, and the cal data recorded prior to each pulsar observation. From residual variation versus hour angle in the calibrated polarization of B1929+10, we infer that the systematic error in the calibration procedure is at most $\sim 5\%$ of the total polarized flux density. For most of our targets this is less than the uncertainty due to noise.

Finally the two sets of calibrated data recorded with different feed angles were averaged to form the final calibrated polarization profiles as a function of frequency. From these data, the RM of each pulsar was obtained, and the polarization data were corrected for Faraday rotation and averaged to form a single polarization profile, integrated over the band.

3. POLARIZATION PROFILES

We observed 100 pulsars with the GBT centered on 774 MHz, including four calibration pulsars. The targets were selected from the set of pulsars in the northern sky with unknown or uncertain rotation measures. For 67 of these pulsars, our observations are the first published polarization measurements. Where possible in this section, the polarization profiles have been grouped and presented according to their main polarization properties. Although each profile is plotted only once, some will be discussed in more than one subsection. We also compare our profiles with previous polarization observations when available.

In Table 1, we list for each source: pulsar J2000 source name, B1950 source name where applicable, spin period (in seconds), dispersion measure (DM, in pc cm^{-3}), and spin-down luminosity (\dot{E} , in erg s^{-1}). These values were obtained from the ATNF pulsar catalog (Manchester et al. 2005). They are followed by our measured parameters at 774 MHz: the observed average flux density S (in mJy), average linearly polarized flux density L (in mJy), average circularly polarized flux density V (in mJy), average absolute circularly polarized flux density $|V|$ (in mJy), as well as the uncertainty of these flux densities, followed by the full pulse width measured at half peak flux density (in degrees). We also give the number of the figure in which the polarization profile is presented, and what previous polarization observations are available.

3.1. Calibration Pulsars

Figure 2 shows polarization profiles of the four pulsars that we observed for calibration purposes, PSRs B1857-26 (J1900-2600), B1900+01 (J1903+0135), B1929+10 (J1932+1059), and B1933+16 (J1935+1616); these appear consistent with those presented in previous publications (see references below).

The bright pulsar PSR B1929+10, a standard polarization calibrator, was observed several times at many parallactic angles. From these observations, we derived the instrumental polarization parameters (van Straten 2004). Consistent with previous observations (e.g., Stinebring et al. 1984b; Gould & Lyne 1998; Stairs et al. 1999), the main pulse of PSR B1929+10 shows more than three components, i.e., two peaks plus unresolved leading shoulders, all highly polarized. The right-hand circular polarization is weak and nulls between the main peak and trailing component. The inter-pulse is almost 100% polarized.

PSR B1900+01 is a bright pulsar with a large DM that was observed to check the order of frequency channels. It has strong left-hand circular polarization but extremely weak linear polar-

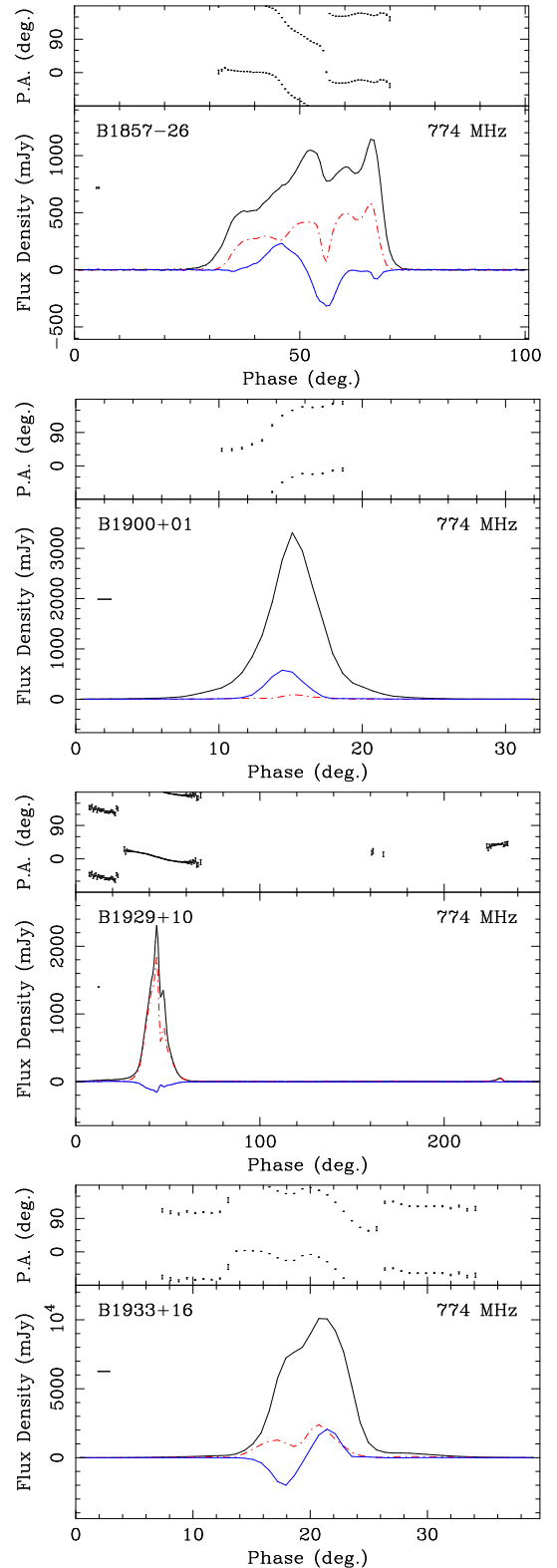


FIG. 2.— Polarization profiles of four strong pulsars observed for calibration purposes. In the lower part of each plot, the upper thick line is the total intensity (Stokes parameter I), the dash-dot-dashed line is the linearly polarized intensity L , and the thin line is the circularly polarized intensity $V = I_L - I_R$, where I_L and I_R are the left and right circularly polarized intensities, respectively. The error box plotted on the left below the pulsar name has a width equal to the pulse-phase instrumental broadening (including dispersion smearing) and a height equal to 4 times the baseline rms noise (i.e. $\pm 2\sigma$). In the upper part, the P.A. angle of the linearly polarized emission is plotted with 2σ error bars only for those phases where the linear polarization is greater than 2σ .

TABLE I
POLARIZATION PARAMETERS OF 100 PULSARS OBSERVED AT 774 MHz BY GBT

PSR Jname	PSR Bname	Period (s)	DM (pc cm ³)	log \dot{E} (erg s ⁻¹)	S	L	V	$ V $	σ	W50 ($^{\circ}$)	Fig.	Notes	Prev.polarization obs. Ref.:Freq.(MHz)
J1900-2600	B1857-26	0.6122	37.99	31.55	78.64	32.81	-0.62	10.21	0.11	26.5	2	cal+cp	See text
J1903+0135	B1900+01	0.7293	245.17	32.61	40.86	0.87	5.16	5.15	0.06	3.8	2	cal	See text
J1932+1059	B1929+10	0.2265	3.18	33.59	61.62	47.39	-4.36	4.84	0.06	9.0	2	cal+hiL	See text
J1935+1616	B1933+16	0.3587	158.52	33.71	266.29	51.10	0.16	39.18	0.14	6.5	2	cal+cp	See text
J0014+4746	B0011+47	1.2407	30.85	31.07	19.87	5.17	-0.67	0.75	0.10	33.4	4	hiL	GL98:610,1418,1642
J0055+5117	B0052+51	2.1152	44.12	31.60	3.66	1.62	0.18	0.20	0.11	10.8	7	db	GL98:408,610,925,1408,1642
J0117+5914	B0114+58	0.1014	49.42	35.34	1.75	0.25	-0.06	0.08	0.08	13.6	9		GL98:408,610,1408
J0156+3949	B0153+39	1.8116	60.00	30.00	0.96	0.38	0.01	0.07	0.10	28.6	9		GL98:606
J0215+6218		0.5489	84.00	32.20	13.08	2.91	0.84	0.94	0.13	26.4	8	ort	
J0415+6954	B0410+69	0.3907	27.46	31.71	1.47	0.13	0.00	0.07	0.10	4.9	9		GL98:408,610,1408
J0849+8028	B0841+80	1.6022	34.66	30.63	1.09	0.38	0.05	0.11	0.08	10.1	9		GL98:606
J0921+6254	B0917+63	1.5680	13.16	31.57	1.58	0.47	-0.06	0.05	0.10	8.0	7	db	GL98:234,410,606,1408
J1012+5307		0.0053	9.02	33.67	3.05	1.78	0.02	0.17	0.07	47.6	3	MSP+hiL	S+99:610;X+98:1410
J1300+1240	B1257+12	0.0062	10.17	34.27	1.34	0.33	0.05	0.19	0.08	39.9	3	MSP+hiL+cp	X+98:1410
J1321+8323	B1322+83	0.6700	13.31	31.87	0.77	0.63	-0.07	0.07	0.08	10.9	4	hiL	GL98:410,606,925,1408
J1453+1902		0.0058	14.05	33.37	0.54	0.25	-0.00	0.03	0.07	21.6	3	MSP	
J1503+2111		3.3140	11.75	29.18	0.70	0.10	0.01	0.04	0.12	4.1	9		
J1518+4904		0.0409	11.61	31.20	8.36	0.74	-1.21	1.26	0.09	38.5	3	MSP+ort	X+98:1410;S+99:1414
J1549+2113		1.2625	24.80	31.23	0.85	0.08	-0.06	0.07	0.09	3.4	9		
J1627+1419		0.4909	33.80	32.12	4.03	0.39	0.17	0.20	0.07	18.3	9		
J1640+2224		0.0032	18.43	33.55	2.40	0.29	0.10	0.16	0.04	20.2	3	MSP	X+98:1410
J1649+2533		1.0153	35.50	31.32	3.89	1.30	-0.07	0.22	0.12	9.0	9		
J1652+2651		0.9158	40.80	31.53	10.79	4.60	-0.60	0.77	0.10	12.6	6	cp	
J1720+2150		1.6157	41.10	30.84	0.76	0.28	0.03	0.09	0.09	13.6	6	cp+db?	
J1741+2758		1.3607	29.30	31.46	1.03	0.16	-0.08	0.11	0.09	8.6	9		
J1746+2245		3.4650	52.00	30.67	1.50	0.38	0.14	0.20	0.11	1.5	7	db?	
J1746+2540		1.0581	51.50	31.54	1.75	0.73	0.11	0.15	0.12	7.6	6	cp	
J1754+5201	B1753+52	2.3914	35.35	30.66	4.35	1.71	-0.42	0.52	0.10	2.7	6	cp	GL98:410,606,1408
J1758+3030		0.9473	34.90	31.52	4.15	0.52	0.06	0.12	0.10	8.9	9		
J1819+1305		1.0604	64.90	31.08	3.99	1.13	-0.04	0.32	0.12	21.8	6	cp	
J1821+1715		1.3667	60.47	31.13	6.78	1.46	-0.13	0.61	0.14	11.0	6	cp	
J1828+1359		0.7416	56.00	31.85	0.69	0.23	0.21	0.21	0.10	6.5	8	ort	
J1838+1650		1.9020	33.90	31.19	1.89	0.49	-0.21	0.21	0.10	2.3	7	db	
J1845+0623		1.4217	113.00	30.88	1.41	0.27	-0.07	0.09	0.14	3.6	9		
J1848+0604		2.2186	242.70	31.13	1.40	0.41	-0.03	0.13	0.15	5.0	6	cp	
J1849+2423		0.2756	62.24	32.46	3.21	1.05	0.16	0.21	0.10	19.4	4	hiL	
J1853+1303		0.0041	30.57	33.71	1.66	0.42	-0.01	0.20	0.10	54.8	3	MSP+cp	
J1859+1526		0.9340	97.45	32.28	0.42	0.10	-0.08	0.09	0.08	—	9		
J1900+0227		0.3743	201.10	33.63	0.93	0.19	-0.12	0.17	0.18	—	9		
J1901-0312		0.3557	106.40	33.30	0.18	0.09	-0.06	0.06	0.11	—	4	hiL?	
J1901+0124		0.3188	314.40	33.60	0.29	0.16	0.07	0.07	0.16	13.2	4	hiL?	
J1902-0340		1.5247	114.00	31.35	0.56	0.10	0.02	0.07	0.10	12.2	9		
J1902+0723		0.4878	105.00	31.85	1.45	0.26	0.27	0.25	0.13	12.7	9		
J1903+0601		0.3741	388.00	34.16	1.03	0.25	-0.02	0.06	0.16	—	9		
J1903+2225		0.6512	109.20	31.80	1.02	0.21	-0.05	0.07	0.10	6.7	9		
J1906+0414		1.0434	349.00	32.60	0.44	0.11	0.04	0.04	0.16	7.1	9		
J1906+0649		1.2866	249.00	30.45	0.98	0.37	0.09	0.12	0.21	—	9		
J1906+1854		1.0191	156.72	30.88	2.47	0.20	0.05	0.18	0.10	23.8	9		
J1907+0345		0.2402	311.70	34.37	0.00	0.00	0.00	0.00	0.14	7.4	4	hiL?	
J1909+0616		0.7560	352.00	33.27	1.90	0.29	0.26	0.29	0.07	18.4	9		
J1909+1450		0.9961	119.50	30.94	0.32	0.15	0.01	0.01	0.14	—	9		
J1909+1859		0.5425	64.48	31.38	1.32	0.47	0.11	0.20	0.13	8.3	9		
J1911+1758		0.4604	48.97	30.72	0.36	0.12	0.01	0.03	0.10	9.3	9		
J1912+1036	B1910+10	0.4093	147.00	33.96	0.21	0.11	-0.03	0.04	0.12	—	4	hiL?	
J1912+2525		0.6220	37.84	31.57	0.74	0.08	-0.07	0.07	0.09	4.5	9		
J1915+0738		1.5427	39.00	31.55	1.47	0.77	-0.31	0.32	0.15	1.9	9		
J1915+0752		2.0583	105.30	29.80	1.45	0.39	-0.08	0.13	0.16	4.3	9		
J1915+0838		0.3428	358.00	33.19	0.85	0.23	0.10	0.10	0.13	16.7	9		
J1920+2650	B1918+26	0.7855	27.62	30.45	5.85	1.47	1.32	1.55	0.13	6.5	5	hiCP+cp+nom	W+99:1400;GL98:410,610,1642

TABLE 1
PARAMETERS OF 100 PULSARS OBSERVED AT 774 MHz BY GBT – CONTINUED

PSR Jname	PSR Bname	Period (s)	DM (pc cm ³)	$\log \dot{E}$ (erg s ⁻¹)	S	L	V	$ V $	σ	W50 (°)	Fig.	Notes	Prev.polarization obs. Ref.:Freq.(MHz)
J1921+2003	B1919+20	0.7607	101.00	30.65	1.49	0.32	-0.27	0.28	0.10	2.7	7	db	W+04:430
J1924+2040	B1922+20	0.2378	213.00	33.79	3.95	0.43	-0.12	0.16	0.11	16.5	9		GL98:610
J1926+1434	B1924+14	1.3249	211.41	30.57	4.04	0.99	-0.32	0.41	0.14	5.2	7	db	RB81:430;GL98:606,1408
J1927+1856	B1925+188	0.2983	99.00	33.52	1.02	0.15	-0.05	0.13	0.08	18.3	9		
J1927+2234	B1925+22	1.4311	180.00	31.02	1.99	0.29	0.07	0.14	0.12	9.4	9		W+99:1400
J1930+1316	B1927+13	0.7600	207.30	32.52	0.69	0.15	-0.02	0.03	0.08	3.2	9		W+04:430;W+99:1400
J1931+1536	B1929+15	0.3144	140.00	33.80	0.50	0.11	-0.01	0.05	0.12	12.4	9		W+04:430
J1933+1304	B1930+13	0.9283	177.90	31.20	1.48	0.40	-0.03	0.16	0.12	10.2	7	db	W+99:1400
J1933+2421	B1931+24	0.8137	106.03	32.77	3.59	1.34	-0.44	0.49	0.09	9.7	6	cp	GL98:410,606
J1936+1536	B1933+15	0.9673	165.00	32.25	0.79	0.23	0.17	0.19	0.10	7.9	9		W+99:1400
J1937+2544	B1935+25	0.2010	53.22	33.50	7.69	2.49	-0.13	0.26	0.11	25.4	7	db+hiL	GL98:606,925,1408,1642; W+99:1400;J+07:691,3100
J1939+2449	B1937+24	0.6453	142.88	33.43	5.77	1.95	0.34	0.46	0.12	10.9	4	hiL+ort	
J1941+1026		0.9054	138.91	31.72	0.75	0.15	-0.06	0.08	0.13	4.7	9		
J1944+1755	B1942+17	1.9969	175.00	30.56	2.25	0.88	-0.11	0.15	0.17	3.4	7	db+hiL	W+04:430
J1945+1834	B1943+18	1.0687	217.70	30.89	0.29	0.02	0.02	0.05	0.12	8.6	9		
J1946+2611		0.4351	165.00	34.02	2.24	0.91	-0.22	0.20	0.12	12.1	9		
J1951+1123		5.0941	31.29	29.96	0.85	0.12	-0.00	0.02	0.11	1.8	9		
J1952+1410	B1949+14	0.2750	31.46	32.39	0.97	0.20	-0.13	0.14	0.09	7.2	9		
J1955+2908	B1953+29	0.0061	104.58	33.71	2.89	0.80	-0.02	0.49	0.07	100.9	3	MSP	X+98:1410;TS90:1400
J1957+2831		0.3077	138.99	33.62	2.76	0.72	-0.07	0.21	0.09	12.0	4	hiL+cp+ort	
J2002+3217	B2000+32	0.6968	142.21	34.09	4.65	1.56	-0.35	0.37	0.13	5.1	9		W+99:1400;HR08:430; GL98:408,610,925,1408,1642
J2008+2513		0.5892	60.55	33.02	3.10	0.92	-0.17	0.19	0.11	7.0	4	hiL+ort	
J2017+2043		0.5371	61.50	32.40	1.31	0.31	-0.00	0.13	0.09	11.3	6	cp+db	
J2023+5037	B2022+50	0.3726	33.02	33.28	7.74	1.65	-0.26	0.36	0.10	4.0	4	hiL+ort	GL98:410,610,925,1408,1642
J2029+3744	B2027+37	1.2168	190.66	32.43	3.59	0.64	-0.25	0.26	0.11	5.3	9		W+99:1400;GL98:410,610,1408,1642
J2037+3621	B2035+36	0.6187	93.56	32.88	9.36	2.69	-0.17	0.22	0.13	10.1	8	nort	GL98:606,1408,1642;W+99:1400
J2038+5319	B2036+53	1.4246	160.10	31.11	1.73	0.51	-0.06	0.21	0.10	5.3	6	cp	GL98:606,1408
J2044+4614		1.3927	315.40	30.96	5.86	1.96	0.06	0.44	0.15	6.4	7	db	
J2046+5708	B2045+56	0.4767	101.81	33.61	1.17	0.55	-0.08	0.09	0.09	9.5	9		GL98:606
J2139+2242		1.0835	44.10	31.64	34.16	14.76	0.79	1.50	0.10	10.4	6	cp	
J2151+2315		0.5935	23.60	32.13	0.39	0.16	0.00	0.13	0.03	192.5	4	hiL?	
J2155+2813		1.6090	77.40	30.94	0.94	0.10	-0.03	0.07	0.09	3.6	9		
J2156+2618		0.4981	48.80	30.66	0.42	0.07	0.03	0.05	0.09	7.1	9		
J2205+1444		0.9380	36.72	31.63	0.84	0.39	0.09	0.09	0.07	18.1	7	db	
J2215+1538		0.3742	29.26	33.25	16.55	5.03	0.10	0.52	0.08	5.0	6	cp	
J2234+2114		1.3587	35.08	30.54	4.30	1.02	0.34	0.38	0.09	21.4	9		
J2235+1506		0.0598	18.09	31.46	1.77	0.21	-0.00	0.11	0.11	16.6	3	MSP	
J2253+1516		0.7922	29.18	30.72	5.65	0.93	-0.27	0.48	0.17	3.1	7	db	
J2302+6028		1.2064	156.70	31.66	9.75	2.78	0.83	0.98	0.11	4.7	9		
J2305+4707	B2303+46	1.0664	62.06	31.27	1.18	0.07	0.11	0.12	0.09	8.2	9		GL98:408,606,1642
J2307+2225		0.5358	7.08	30.35	3.65	1.79	0.19	0.20	0.15	5.6	9		

1) The pulsar spin period (in seconds), dispersion measure (DM, in pc cm⁻³) and spin-down luminosity (\dot{E} , in erg s⁻¹) were taken from the pulsar catalog (Manchester et al. 2005). The newly observed average flux density S at 774 MHz, average linearly polarized flux density L , average circularly polarized flux density V , average absolute circularly polarized flux density $|V|$, as well as the uncertainty of these flux densities, are all in mJy. The full pulse width measured at half peak flux is in degrees of rotational phase.

2) Notes: MSP: millisecond pulsar; hiL: high linear polarization; hiCP: high circular polarization; cp: circular polarization with sense reversal; db: double components; ort: orthogonal modes; nort: non-orthogonal modes.

3). References for previous polarization observations: GL98: Gould & Lyne (1998); HR08: Hankins & Rankin (2008); J+07: Johnston et al. (2007); RB81: Rankin & Benson (1981); S+99: Stairs et al. (1999); TS90: Thorsett & Stinebring (1990); W+99: Weisberg et al. (1999); W+04: Weisberg et al. (2004); X+98: Xilouris et al. (1998).

ization. The polarization profile is consistent with that given by GL98.

PSRs B1933+16 and B1857–26 were also observed to validate the phase convention of the instrument, which affects the handedness of circular polarization as well as the position angle. The polarization profile of PSR B1933+16 at 774 MHz has two barely resolvable components with reversed circular polarization, similar to those at 925 MHz (see Gould & Lyne 1998, hereafter GL98) and 1400 MHz (Rankin et al. 1989; Weisberg et al. 1999). The P.A. values of this pulsar at 774 MHz also compare well with those at 1.4 GHz given by Johnston et al. (2005) and are consistent with the small RM ($= -1.9 \text{ rad m}^{-2}$) of this pulsar. Our observations of PSR B1857–26 at 774 MHz have better sensitivity than previously published data at 610 MHz, 800 MHz and 925 MHz (van Ommen et al. 1997; Manchester et al. 1998, GL98). All profiles at these frequencies show consistent linear and circular polarization.

3.2. Millisecond pulsars

The eight millisecond pulsars that we observed are shown in Figure 3.

PSR J1012+5307 has emission at almost all longitudes and appears to have three main regions of emission. Two and a half of these are 100% linearly polarized, confirming the observations at 610 MHz by Stairs et al. (1999) and at 1.41 GHz by Xilouris et al. (1998). Note that the PA convention in Stairs et al. (1999) is different from other pulsar polarization observations. We did not detect much circular polarization at 774 MHz, in contrast with Stairs et al. (1999) and Xilouris et al. (1998).

PSR B1257+12 (J1300+1240) has a 100% linearly polarized leading edge, confirming the measurements at 1.41 GHz by Xilouris et al. (1998). However, our observations indicate a reversal from right to left circular polarization in the leading half of the profile, and the circular polarization at 1.4 GHz in Xilouris et al. (1998) is very different from our data (see comments at the end of Manchester & Han 2004).

PSR J1518+4904 has right-hand circular polarization at 774 MHz for almost the full profile, rather than just the first half of the profile, as observed at 1.41 GHz by Xilouris et al. (1998) and Stairs et al. (1999).

Observations of PSR J1640+2224 show weak linear polarization and very weak circular polarization at 774 MHz, in contrast to the high linear and circular polarization at 1.41 GHz reported by Xilouris et al. (1998).

At 774 MHz, PSR B1953+29 (J1955+2908) shows observable linear polarization in the stronger trailing component. Circular polarization is almost undetectable anywhere in the profile, which is consistent with the result at 1.41 GHz reported by Thorsett & Stinebring (1990) but in contrast to the strong right circular polarization of the leading component observed at the same frequency by Xilouris et al. (1998).

PSRs J1453+1902, J1853+1303, and J2235+1506 have never been observed before. Our GBT 774 MHz data show strong linear polarization of the former two and weak polarization of the latter one, though the total signal-to-noise ratio (S/N) is not very high.

We see from our observations that the profiles of millisecond pulsars are very wide, with their W_{50} values among the highest (see Table 1 and Figure 3). Second, the P.A. curves of all millisecond pulsars are rather flat where measurable (see Figure 3).

3.3. Profiles with Highly Linearly Polarized Emission

Many pulsars in our data set show highly linearly polarized emission (indicated by “hiL” in Table 1) for all or part of their profiles (Figure 4).

Five or six pulsars, PSRs B1322+83 (J1321+8323), J1901+0124, J1901–0312, J1907+0345, B1910+10 (J1912+1036), and perhaps also PSR J2151+2315 appear to have a single dominant component with up to 100% linear polarization. Of these pulsars, only PSR B1322+83 (J1321+8323) was previously observed; our GBT observation at 774 MHz is consistent with those of GL98 (at 410, 606, 925, and 1408 MHz). The linear polarization percentage drops from 100% at 410 MHz to 50% at 1408 MHz, and the whole profile is right-hand circularly polarized. The precursor is clearly visible at 606 MHz but only marginally detected around the phase of 35° at 774 MHz in our Figure 4.

A number of pulsars exhibit nearly 100% linear polarization at 774 MHz in only the leading or trailing edge of the pulse profile; for example, the bottom six pulsars in Figure 4, PSR B1929+10 in Figure 2, two millisecond pulsars, PSRs J1012+5307 and B1257+12 (J1300+1240) in Figure 3, and two double component pulsars, PSRs B1935+25 (J1937+2544) and B1942+17 (J1944+1755) in Figure 7. PSR B0011+47 (J0014+4746) was previously observed by GL98 at 404, 610, 925, 1414, and 1642 MHz. Our GBT observation at 774 MHz has high S/N and for the first time clearly shows the 100% linearly polarized leading edge. The interpulse pulsar PSR B2022+50 (J2023+5037) has been observed by GL98 at 410, 610, 925, 1408, and 1642 MHz. Our GBT observation has the best S/N, and clearly shows both the orthogonal mode of the main pulse and the 100% linear polarization of the leading edge of the interpulse. PSR B1935+25 (J1937+2544) in Figure 7 shows 100% linear polarization in the trailing edge of the leading component; another double component pulsar, PSR B1942+17 (J1944+1755) (Figure 7) exhibits highly linearly polarized emission in the bridge.

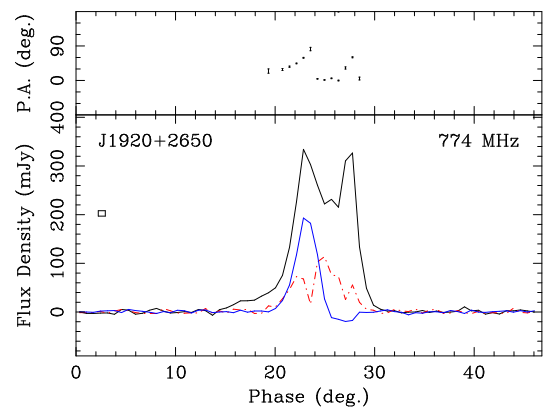


FIG. 5.— PSR B1918+26 (J1920+2650) shows extremely strong circular polarization. See keys in Figure 2.

3.4. Highly Circular Polarized Component

The average pulse profiles of most pulsars exhibit relatively weak circular polarization. Therefore, in our sample, PSR B1918+26 (J1920+2650, see Figure 5) is outstanding for the strong left-hand circular polarization observed in its first major component, with fractional circular polarization reaching 64%. Observations at 1.4 GHz (Weisberg et al. 1999) and at 610 MHz (GL98) also show extraordinarily high circular polarization in this component. Similar characteristics have been previously

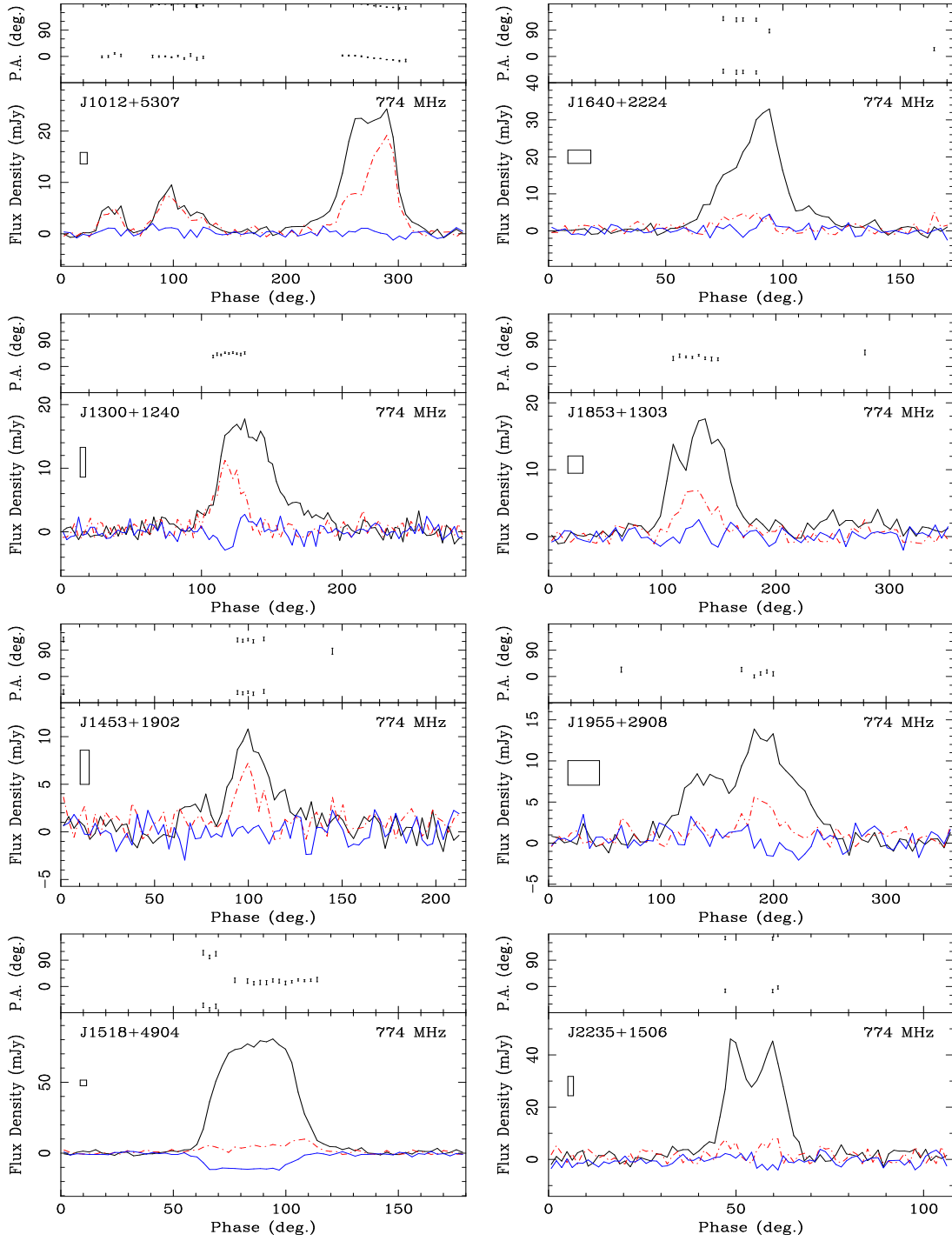


FIG. 3.— Polarization profiles of 8 millisecond pulsars. See keys in Figure 2

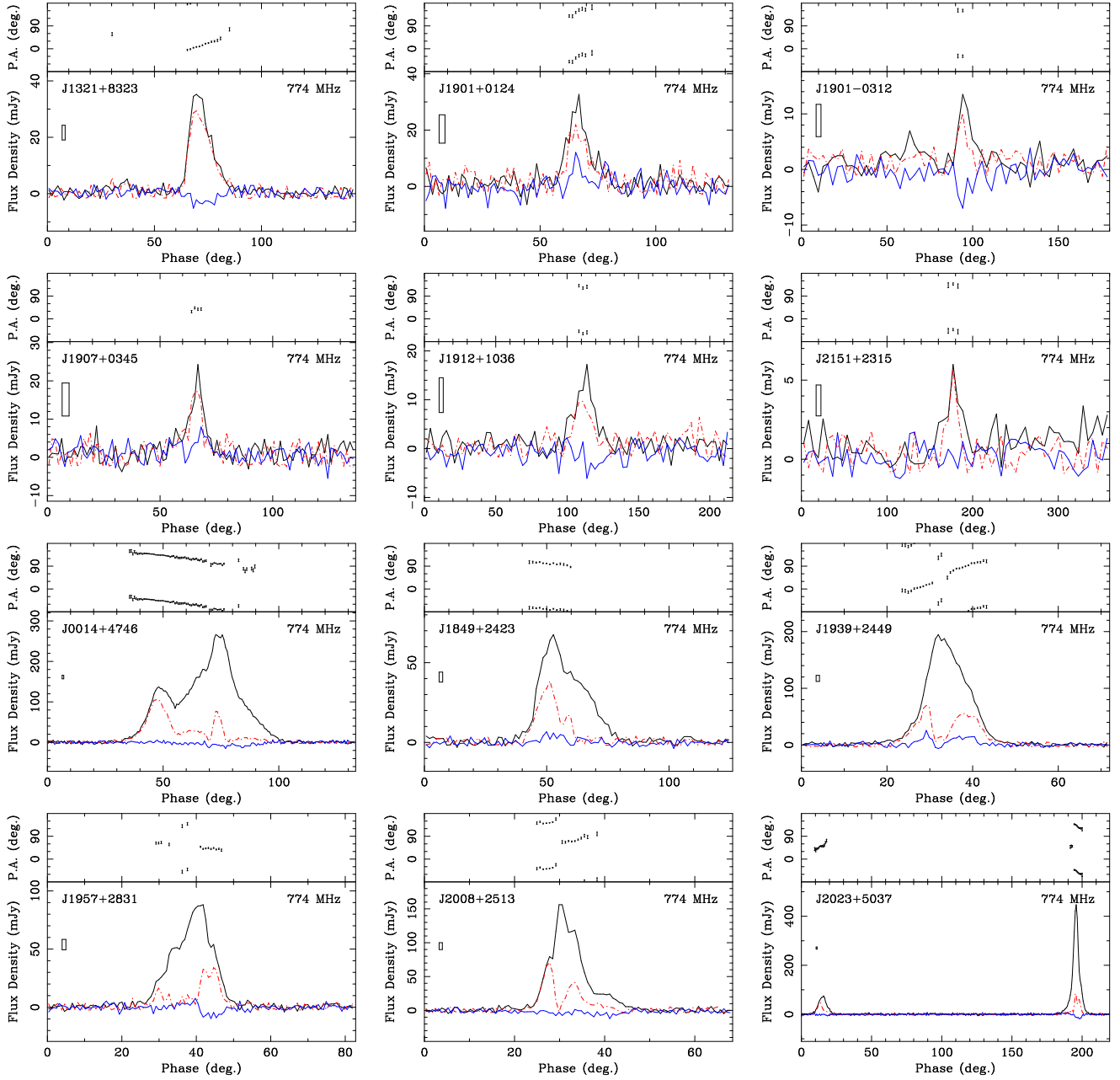


FIG. 4.— Top six pulsars have nearly 100% polarization (linear plus circular) across the entire pulse profile, and the bottom six pulsars have nearly 100% linear polarization for parts of their profiles. See keys in Figure 2. Other pulsars belonging to this category are PSR B1929+10 in Figure 2, PSRs J1012+5307 and B1257+12 (J1300+1240) in Figure 3, and PSRs B1935+25 (J1937+2544) and B1942+17 (J1944+1755) in Figure 7.

observed in very few other pulsars, notably PSRs B1702–19 (Lyne & Manchester 1988), J1603–7202 (Manchester & Han 2004) and J1907+0918 (Lorimer & Xilouris 2000). This is only the fourth case of fractional circular polarization exceeding 50% in any component of a mean pulse profile.

3.5. Sense Reversal of Circular Polarization

Many pulsars show sense reversal of circular polarization as a function of pulse phase. Together with the steepness of the polarization angle curve, this is an important feature for identifying the core emission component (Rankin 1983; Radhakrishnan & Rankin 1990; Rankin 1990). The core component is located near the center of an emission beam, and sometimes has an offset toward a later longitude due to a retardation effect (Xu et al. 1997; Gupta & Gangadhara 2003). Similar reversal of the sense of circular polarization is observed in many of the pulsars in our sample, as shown in Figure 6.

The sense reversal of circular polarization of the first six pulsars in the upper part of Figure 6 and PSR J1957+2831 in Figure 4 is probably associated with an either unresolved or marginally resolved core component near the pulse center. Three pulsars, PSRs J1652+2651, B1931+24 (J1933+2421), J2215+1538, and also PSR B1919+26 (J1920+2650) in Figure 5, show a sense reversal from a component located at a later longitude than the pulsar center, which probably is not core emission, except for B1931+24. The sense reversals of another three pulsars, PSRs J1848+0604, B2036+53 (J2038+5319), and J2139+2242, as well as the millisecond pulsar PSR J1300+1240, happen at an earlier longitude than the pulse center and do not originate from core emission. The sense reversal in PSR B2036+53 (J2038+5319) is associated with the component peak, but two reversals of PSR J2139+2242 are located between two or three unresolved components, very similar to the case of the calibration pulsar PSR B1933+16.

3.6. Double Component Pulsars

Many pulsars show dominant double-peaked components (Figure 7) that, in some cases, originate from the (possibly single outer) conal emission beam. These are the classical *conal-double* pulsars which are also characterized by the “S” shape of polarization angle (PA) curves (Rankin 1983). Strong correlation between the senses of PA variation and the handedness of circular polarization has been found for conal double pulsars by Han et al. (1998). Decreasing P.A. curves are associated with left hand (positive Stokes V) circular polarization, and increasing P.A. curves with right-hand circular polarization. See You & Han (2006) for updates. Below, we discuss whether the conal-double pulsars in our sample follow this correlation.

We have observed many double-component pulsars (see Figure 7). Not all double-component pulsars are conal-double in nature; for example, most of the double-peak pulsars discussed by Johnston & Weisberg (2006) are not conal-double pulsars. In our observations, PSRs B1935+25 (J1937+2544) and J2253+1516 have double peaks but, with a fast P.A. sweep and even orthogonal polarization modes, the second peak of PSR B1935+25 and the first peak of PSR J2253+1516 (see Figure 7) look more like core components. The polarization observation at 691 MHz by Johnston et al. (2007) not only confirms our profile at 774 MHz, but also shows up to three unresolved components in the second peak of PSR B1935+25. The leading two separate and the trailing one disappears at 3100 MHz (Johnston et al. 2007). Therefore, PSRs B1935+25 and J2253+1516 likely belong to the par-

tial cone class (Lyne & Manchester 1988).

The remaining ten pulsars in Figure 7 are possible conal-double pulsars, with a few questionable cases such as the strange P.A. curves of PSRs J1838+1650 and J2044+4614 and the very weak detection of circular polarization from PSRs B1942+17 (J1944+1755) and J2044+4614. We found that PSRs B0052+51 (J0055+5117) and J2205+1444 have a decreasing P.A. and weak left-hand (positive) circular polarization. PSRs B0917+63 (J0921+6254), J1838+1650, B1924+14 (J1926+1434), and B1942+17 (J1944+1755) have an increasing P.A. and right-hand (negative) circular polarization. These six pulsars agree with the previously observed correlation between the P.A. curve slope and circular polarization sense; however, three other pulsars do not comply with the correlation. PSR J1746+2245 shows an increasing P.A. curve but left-hand circular polarization. PSRs B1919+20 (J1921+2003) and B1930+13 (J1933+1304) have right-hand circular polarization, but their P.A. curves seem to decrease.

PSR B0052+51 (J0055+5117) was included in the updated list of conal-double pulsars in Table 4 of You & Han (2006) according to data by GL98. A possible core component hinted by 408 MHz data (GL98) is unrecognizable in our 774 MHz profile.

PSR B0917+63 (J0921+6254) was observed by GL98 below 1.4 GHz. Our GBT data have better S/N, and confirm that it is a conal double with clear increasing P.A. swing and weak right-hand circular polarization.

3.7. Orthogonal Modes

Radio pulsar emission at a given rotational phase may be an incoherent sum of orthogonally polarized modes. These modes may be generated in one region, one with P.A. parallel and one perpendicular to the magnetic field. It is also possible that the modes come from different emission regions and hence different PAs may appear at a given pulse longitude, producing nonorthogonal modes (e.g., Xu et al. 1997). The orthogonal polarization modes or superposition of emission from two regions leads to complicated PA curves in the integrated profiles. The typical signature of this effect is a sudden $\sim 90^\circ$ jump in P.A. at a certain pulse phase, accompanied by a reduction in the degree of linear polarization.

Many of the targets that we observed show evidence for orthogonal modes in their P.A. curves: PSRs B1929+10, B1933+16, B1857-26 (Figure 2), J0215+6218 (Figure 8), J1518+4904 (Figure 3), J1828+1359 (Figure 8), B1937+24 (J1939+2449), J1957+2831, J2008+2513, B2022+50 (J2023+5037) (Figure 4), and J2253+1515 (Figure 7). We also note that the P.A. curves of PSRs B1918+26 (J1920+2650, Figure 5) and B2035+36 (J2037+3621, Figure 8) may result from nonorthogonal emission modes. Our observation of PSR B2035+36 (J2037+3621) has a better S/N than those at 1.41 GHz by Weisberg et al. (1999) and 606, 925, 1408 and 1642 MHz by GL98.

3.8. Other Pulsars

Our GBT observations of the remaining pulsars in Figure 9 are mostly new polarization measurements. Only a few pulsars in this set have been observed before (Weisberg et al. 1999; Weisberg et al. 2004, GL98), and our GBT data generally have better S/N. The polarization profile of PSRs B0114+58 (J0117+5914) and B1927+13 (J1930+1316) at 430 MHz (Weisberg et al. 2004, GL98) is similar to our 774 MHz profile. PSR B2027+37 (J2029+3744) has been observed at 1.4 GHz by Weisberg et al. (1999) and 410, 610, 1408 and 1642 MHz by GL98. Our polarization

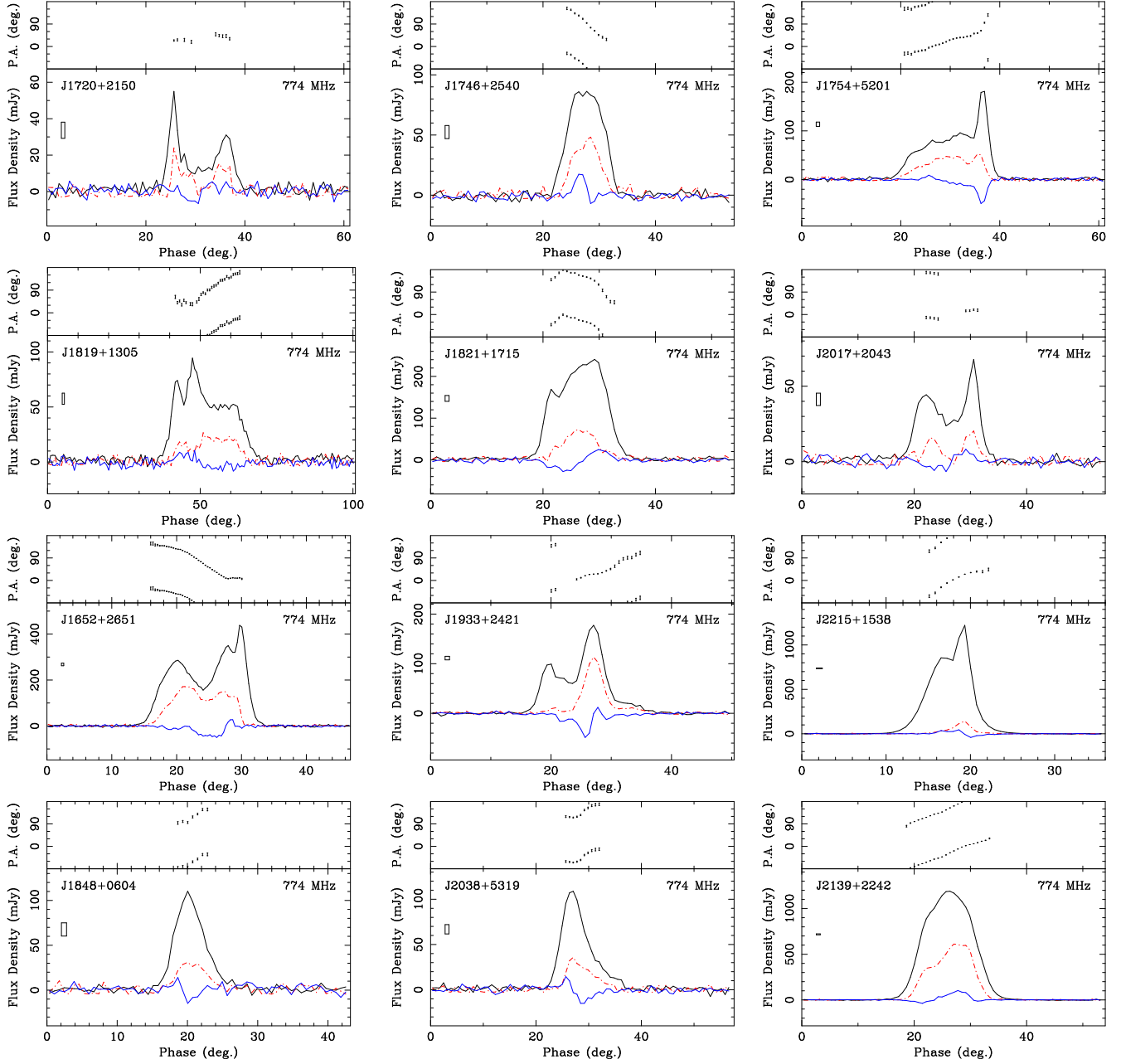


FIG. 6.— These pulsars, together with PSRs B1933+16 and B1857–26 (J1900–2600) in Figure 2, PSR B1257+12 (J1300+1240) in Figure 3, PSR J1957+2831 in Figure 4 and PSR B1918+26 (J1920+2650) in Figure 5, show clear reversals of circular polarization sense. See keys in Figure 2. The top six pulsars show the sense reversal at the pulse center, the next three pulsars have a reversal in a component at a later longitude, and the bottom three pulsars have a reversal at an earlier longitude.

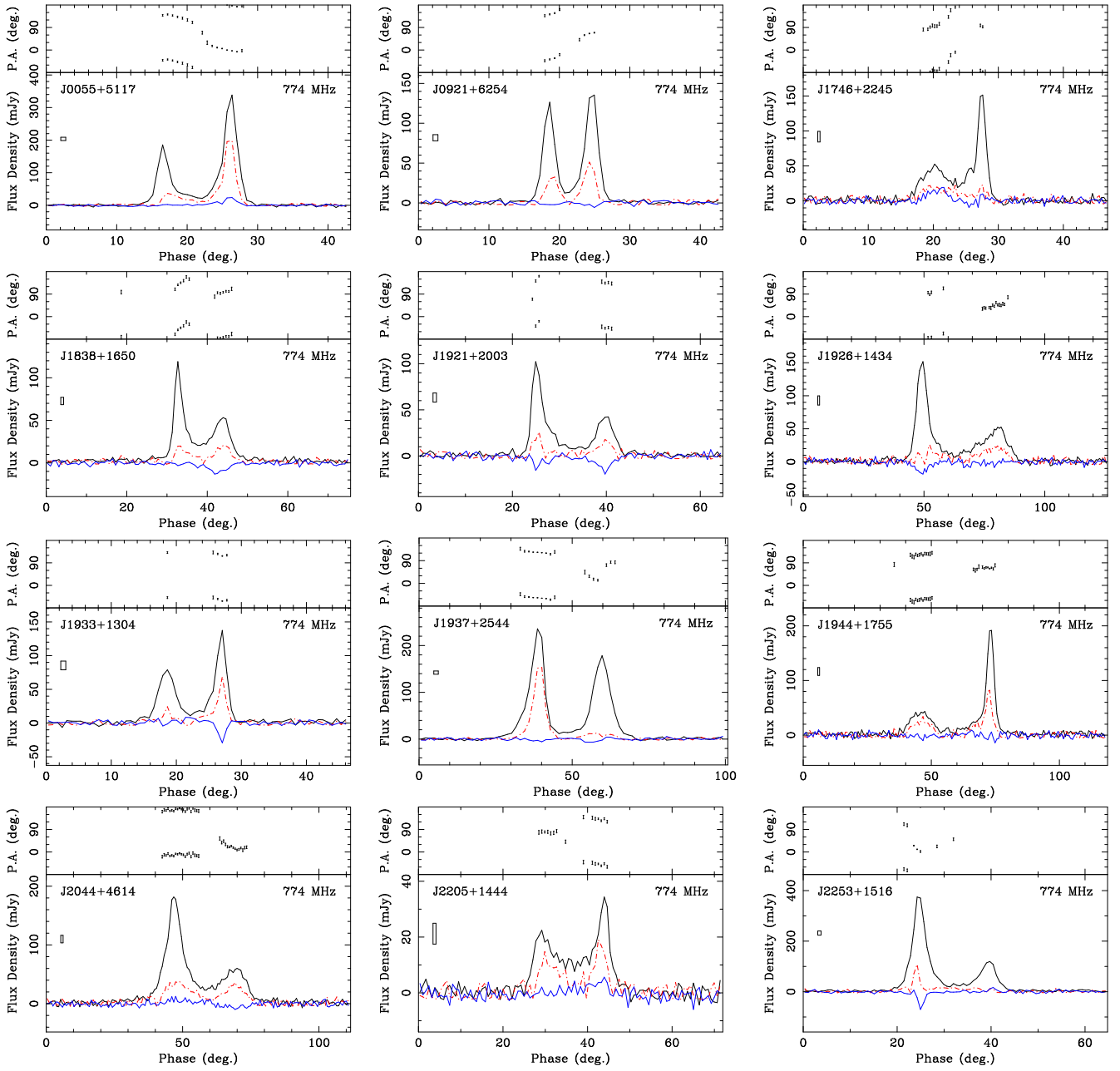


FIG. 7. — Polarization profiles of double-component pulsars at 774 MHz. PSR J2017+2043 in Figure 6 is a double-component pulsar as well. Some of these pulsars are classical *conal-double* pulsars.

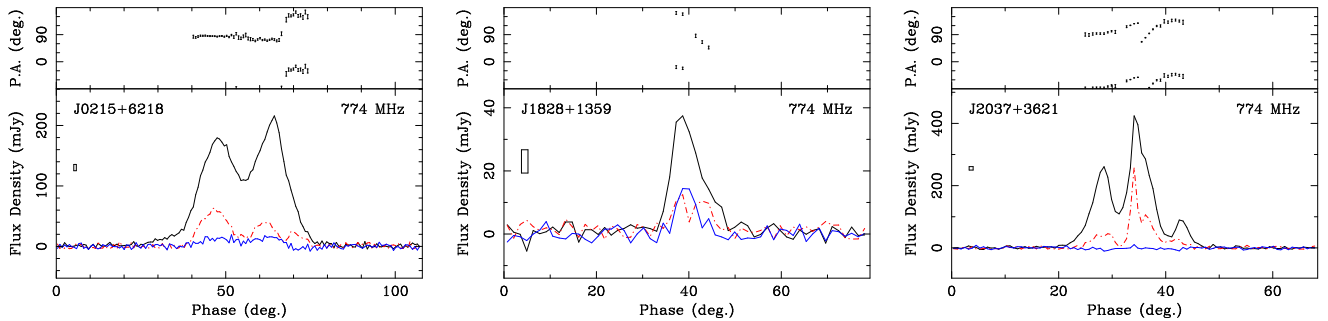


FIG. 8. — These three pulsars show sudden mode jumps in polarization angle curves, as discussed in the text. PSR B2035+36 (J2037+3621) appears to have a nonorthogonal mode jump.

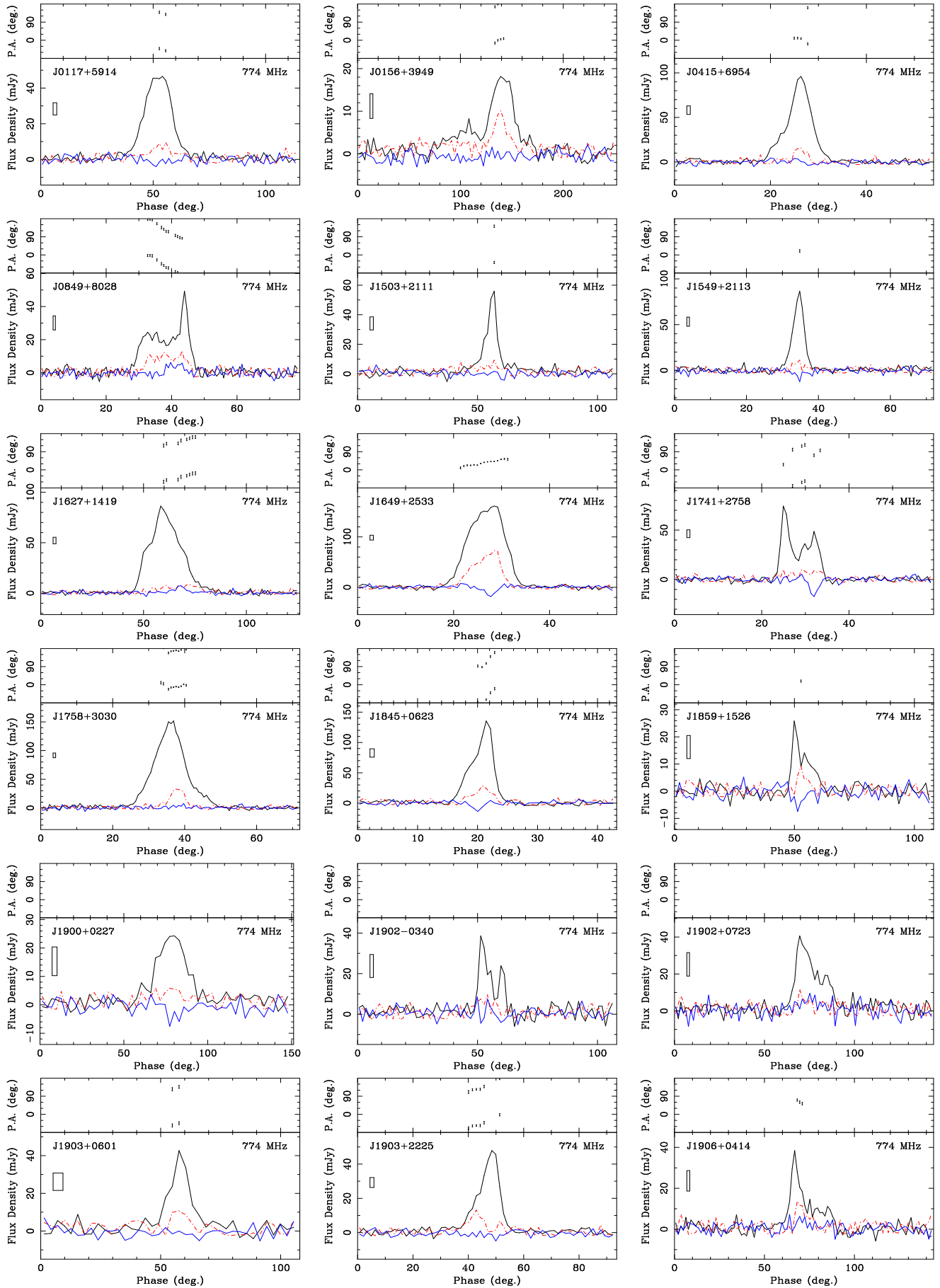


FIG. 9.— Polarization profiles of 51 pulsars at 774 MHz – to be continued.

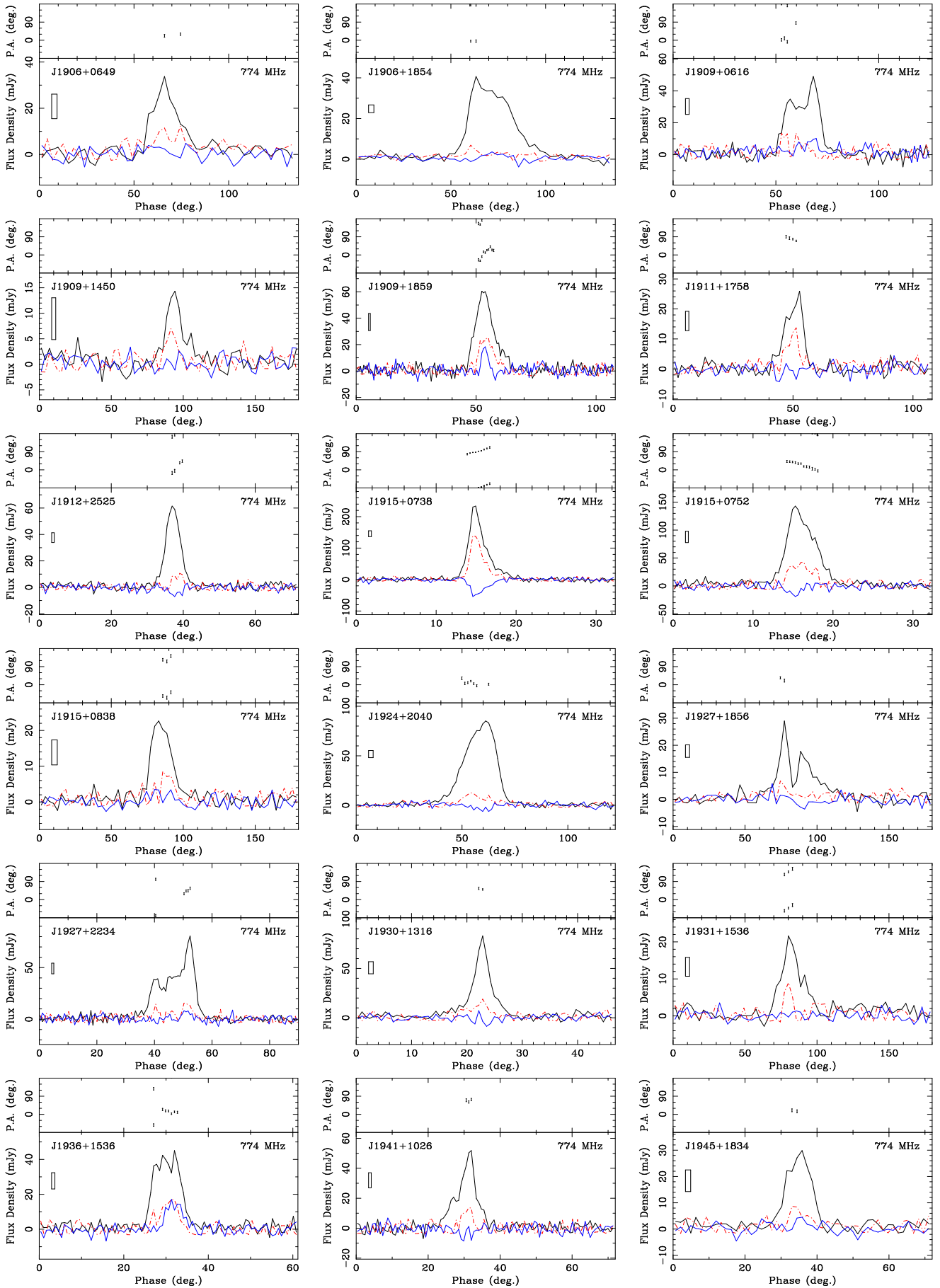


FIG. 9.— Polarization profiles of 51 pulsars at 774 MHz – to be continued.

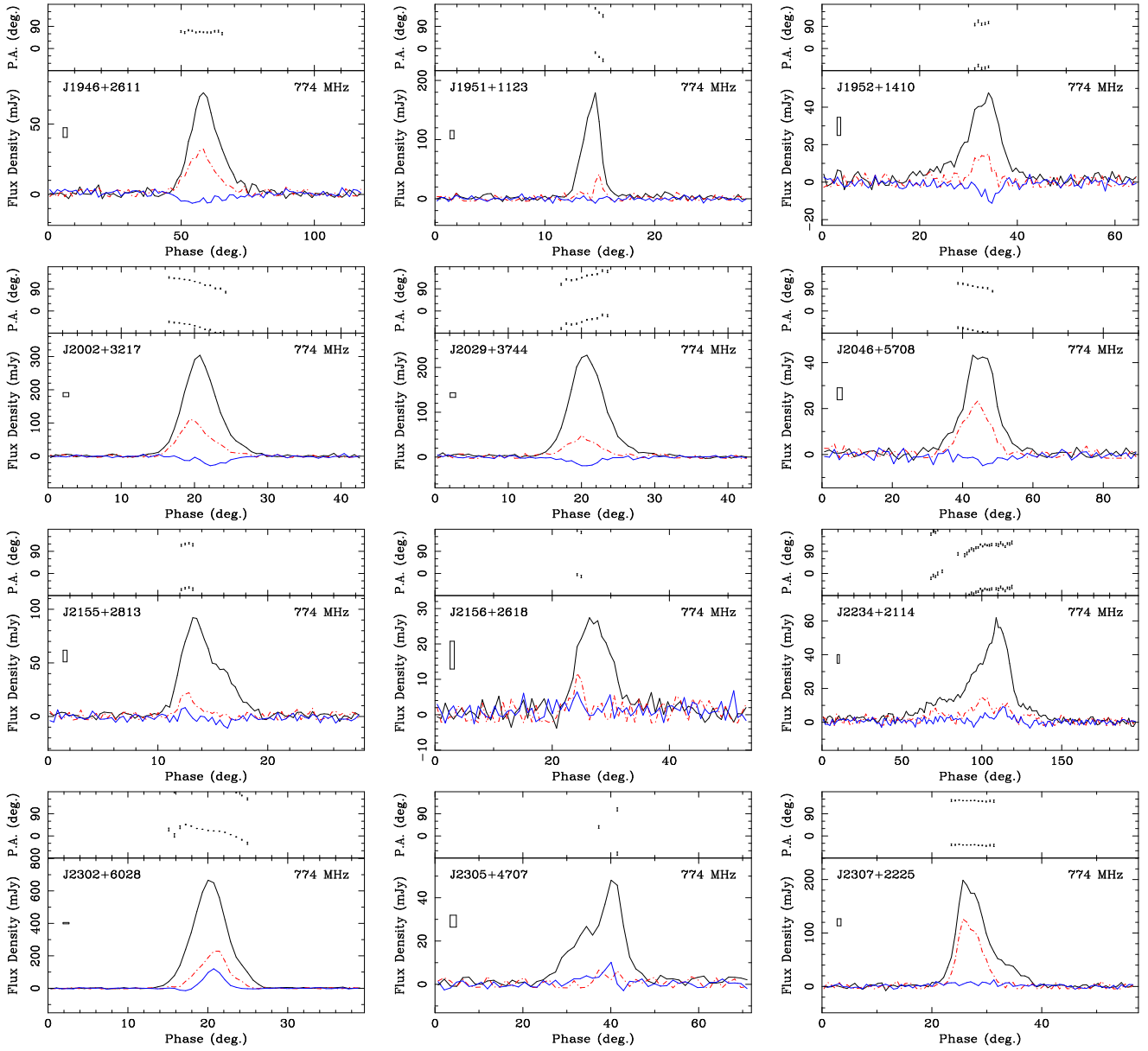


FIG. 9.— Polarization profiles of 51 pulsars at 774 MHz – end.

profile is consistent with the 610 MHz data. Our GBT observations of PSRs B0153+39 (J0156+3949) and B2045+56 (J2046+5708) confirm the linear polarization and P.A. at 606 MHz by GL98.

4. SUMMARY AND DISCUSSIONS

We have observed 100 pulsars using the GBT in order to obtain their polarization profiles at 774 MHz. These are the first published polarization measurements for 67 of them. Our observations consistently provide better quality profiles for pulsars which have been previously observed. The polarization properties of 7 millisecond pulsars in our sample show wide profiles and flat P.A. curves. We also detected extremely strong linear polarization from six pulsars. Together with circular polarization, they are almost 100% polarized over the whole pulse. About a dozen pulsars have almost 100% linear polarization for only a small part of their pulse phase. Extremely strong circular polarization has been detected from one component of PSR J1920+2650. Reversals in the sense of circular polarization have been observed in about 20 pulsars. In only about half of these cases is it associated with the core emission near the pulse center, and in some it is definitely associated with a conal emission component. Most of the observed double-component pulsars are probably conal-double. The correlation between the direction of the P.A. curve and the sense of circular polarization is not statistically significant in our data, likely due to the smaller sample size available here than was used in Han et al. (1998) and You & Han (2006). Because the circular polarization of some pulsars evolves with frequency (see Han et al. 1998; You & Han 2006) and often may have a transit of handedness near 800 MHz, it may be worth further investigating the dependence of the correlation with frequency in the future.

Another important issue is the relationship between the spin-down luminosity ($\dot{E} = 3.95 \times 10^{46} \text{ erg s}^{-1} \dot{P} P^{-3}$, derived from the pulsar spin period P and period derivative \dot{P}) and the observed percentage of linear polarization. It has been found that pulsars with high \dot{E} tend to have stronger linear polar-

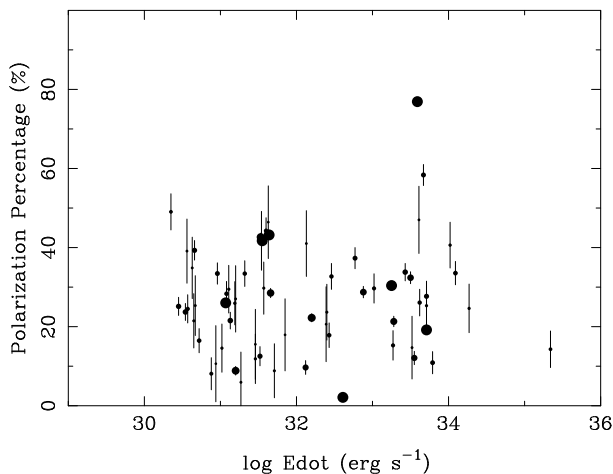


FIG. 10.— Polarization percentage at 774 MHz vs. spin-down luminosity, \dot{E} . The values of \dot{E} were obtained from the ATNF pulsar catalog (Manchester et al. 2005) and also appear in Table 1. Here, only pulsars from our observed sample with an uncertainty of polarization percentage less than 10% are plotted. There is no evidence for correlation between the degree of linear polarization and \dot{E} . The size of the black dots in this plot is inversely proportional to the square root of the uncertainty in polarization percentage, so that the highest quality data clearly stand out.

ization, at least at 1400 MHz (von Hoensbroech et al. 1998; Crawford et al. 2001). We have examined our polarization percentage data at 774 MHz, see Figure 10. Although on average the polarization percentage for pulsars with $\dot{E} > 10^{33} \text{ erg s}^{-1}$ may be slightly larger than that for pulsars with $\dot{E} < 10^{33} \text{ erg s}^{-1}$, the dependence is not significant. Any relationship here is much less prominent than that at 1400 MHz (Crawford & Tiffany 2007). Note also that some highly polarized pulsars in our sample do not have very large \dot{E} .

ACKNOWLEDGMENTS

We thank Professor Don Backer and Professor Ingrid Stairs for use of the GASP pulsar backend and the referee for a very careful review of the manuscript. GBT observations were performed under proposal number GBT07A-024. We sincerely thank Bryan Jacoby for kind contributions to the original observing proposal. J.L.H. is supported by the National Natural Science Foundation (NNSF) of China (10521001, 10773016, and 10833003) and the National Key Basic Research Science Foundation of China (2007CB815403). P.B.D. is a Jansky Fellow of the National Radio Astronomy Observatory. *Facility:* GBT

REFERENCES

- Baars, J. W. M., Genzel, R., Pauliny-Toth, I. I. K., & Witzel, A. 1977, *A&A*, 61, 99
- Cheng, K. S., Ho, C., & Ruderman, M. 1986, *ApJ*, 300, 500
- Cordes, J. M., Rankin, J. M., & Backer, D. C. 1978, *ApJ*, 223, 961
- Crawford, F., Manchester, R. N., & Kaspi, V. M. 2001, *AJ*, 122, 2001
- Crawford, F. & Tiffany, C. L. 2007, *AJ*, 134, 1231
- Demorest, P. B. 2007, PhD thesis, University of California, Berkeley
- Dyke, J., Zhang, B., & Gil, J. 2005, *ApJ*, 626, L45
- Edwards, R. T. & Stappers, B. W. 2004, *A&A*, 421, 681
- Ferdman, R. D., Stairs, I. H., Backer, D. C., Ramachandran, R., Demorest, P., Nice, D. J., Lyne, A. G., Kramer, M., Lorimer, D., McLaughlin, M., Manchester, D., Camilo, F., D’Amico, N., Possenti, A., Burgay, M., Joshi, B. C., & Freire, P. C. 2004, *AAS Abstracts*, 205, 111.01
- Gangadhara, R. T. & Gupta, Y. 2001, *ApJ*, 555, 31
- Gil, J. 1991, *A&A*, 243, 219
- Gould, D. M. & Lyne, A. G. 1998, *MNRAS*, 301, 235
- Gupta, Y. & Gangadhara, R. T. 2003, *ApJ*, 584, 418
- Han, J. L. & Manchester, R. N. 2001, *MNRAS*, 320, L35
- Han, J. L., Manchester, R. N., Lyne, A. G., Qiao, G. J., & van Straten, W. 2006, *ApJ*, 642, 868
- Han, J. L., Manchester, R. N., Xu, R. X., & Qiao, G. J. 1998, *MNRAS*, 300, 373
- Han, J. L., van Straten, W., Manchester, R. N., & Demorest, P. 2009, *ApJ*, in preparations
- Hankins, T. H., Rankin, J. M., 2008, *ApJS*, submitted
- Hotan, A. W., van Straten, W., & Manchester, R. N. 2004, *PASA*, 21, 302
- Johnston, S., Hobbs, G., Vigeland, S., Kramer, M., Weisberg, J. M., & Lyne, A. G. 2005, *MNRAS*, 364, 1397
- Johnston, S., Kramer, M., Karastergiou, A., Hobbs, G., Ord, S., & Wallman, J. 2007, *MNRAS*, 381, 1625
- Johnston, S. & Weisberg, J. M. 2006, *MNRAS*, 368, 1856
- Karastergiou, A. & Johnston, S. 2007, *MNRAS*, 380, 1678
- Kramer, M. 1994, *A&AS*, 107, 527
- Kramer, M., Xilouris, K. M., Lorimer, D. R., Doroshenko, O., Jessner, A., Wielebinski, R., Wolszczan, A., & Camilo, F. 1998, *ApJ*, 501, 270
- Lorimer, D. R. & Xilouris, K. M. 2000, *ApJ*, 545, 385
- Lyne, A. G. & Manchester, R. N. 1988, *MNRAS*, 234, 477
- Lyne, A. G. & Smith, F. G. 1968, *Nature*, 218, 124
- Manchester, R. N. 1996, in *Pulsars: Problems and Progress*, IAU Colloquium 160, ed. S. Johnston, M. A. Walker, & M. Bailes (San Francisco: Astronomical Society of the Pacific), 193
- Manchester, R. N. & Han, J. L. 2004, *ApJ*, 609, 354
- Manchester, R. N., Han, J. L., & Qiao, G. J. 1998, *MNRAS*, 295, 280
- Manchester, R. N., Hobbs, G. B., Teoh, A., & Hobbs, M. 2005, *AJ*, 129, 1993
- McKinnon, M. M. 2004, *ApJ*, 606, 1154
- McKinnon, M. M. & Stinebring, D. R. 2000, *ApJ*, 529, 435
- Navarro, J., Manchester, R. N., Sandhu, J. S., Kulkarni, S. R., & Bailes, M. 1997, *ApJ*, 486, 1019
- Ord, S. M., van Straten, W., Hotan, A. W., & Bailes, M. 2004, *MNRAS*, 352, 804

- Qiao, G. J., Lee, K. J., Wang, H. G., Xu, R. X., & Han, J. L. 2004, *ApJ*, 606, L49
- Radhakrishnan, V. & Cooke, D. J. 1969, *Astrophys. Lett.*, 3, 225
- Radhakrishnan, V. & Rankin, J. M. 1990, *ApJ*, 352, 258
- Rankin, J. M. 1983, *ApJ*, 274, 333
- . 1990, *ApJ*, 352, 247
- . 1993, *ApJ*, 405, 285
- Rankin, J. M. & Benson, J. M. 1981, *AJ*, 86, 418
- Rankin, J. M., Stinebring, D. R., & Weisberg, J. M. 1989, *ApJ*, 346, 869
- Ruderman, M. A. & Sutherland, P. G. 1975, *ApJ*, 196, 51
- Stairs, I. H., Thorsett, S. E., & Camilo, F. 1999, *ApJS*, 123, 627
- Stinebring, D. R., Cordes, J. M., Rankin, J. M., Weisberg, J. M., & Boriakoff, V. 1984a, *ApJS*, 55, 247
- Stinebring, D. R., Cordes, J. M., Weisberg, J. M., Rankin, J. M., & Boriakoff, V. 1984b, *ApJS*, 55, 279
- Thorsett, S. E. & Stinebring, D. R. 1990, *ApJ*, 361, 644
- van Ommen, T. D., D'Alessandro, F. D., Hamilton, P. A., & McCulloch, P. M. 1997, *MNRAS*, 287, 307
- van Straten, W. 2004, *ApJS*, 152, 129
- von Hoensbroech, A., Kijak, J., & Krawczyk, A. 1998, *A&A*, 334, 571
- Weisberg, J. M., Cordes, J. M., Kuan, B., Devine, K. E., Green, J. T., & Backer, D. C. 2004, *ApJS*, 150, 317
- Weisberg, J. M., Cordes, J. M., Lundgren, S. C., Dawson, B. R., Despotes, J. T., Morgan, J. J., Weitz, K. A., Zink, E. C., & Backer, D. C. 1999, *ApJS*, 121, 171
- Xilouris, K. M., Kramer, M., Jessner, A., von Hoensbroech, A., Lorimer, D., Wielebinski, R., Wolszczan, A., & Camilo, F. 1998, *ApJ*, 501, 286
- Xu, R. X., Qiao, G. J., & Han, J. L. 1997, *A&A*, 323, 395
- You, X.-P. & Han, J.-I. 2006, *ChJAA*, 6, 237
- Zhang, B. & Harding, A. K. 2000, *ApJ*, 535, L51